

Actin stress fibers transmit and focus force to activate mechanosensitive channels

Kimihide Hayakawa¹, Hitoshi Tatsumi^{1,2} and Masahiro Sokabe^{1,2,3,*}

¹Cell Mechano-sensing Project ICORP/SORST, Japan Science and Technology Agency, and ²Department of Physiology, Nagoya University Graduate School of Medicine, 65 Tsurumai Showa-ku, Nagoya 468-8550, Japan

³Department of Molecular Physiology, National Institute for Physiological Sciences, NINS, Myodaiji, Okazaki 444-8585, Japan

*Author for correspondence (e-mail: msokabe@med.nagoya-u.ac.jp)

Accepted 19 November 2007

Journal of Cell Science 121, 496-503 Published by The Company of Biologists 2008
doi:10.1242/jcs.022053

Summary

Mechanosensitive (MS) channels are expressed in various cells in a wide range of phylogenetic lineages from bacteria to humans. Understanding the molecular and biophysical mechanisms of their activation is an important research pursuit. It is controversial whether eukaryotic MS channels need accessory proteins – typically cytoskeletal structures – for activation, because MS channel activities are modulated by pharmacological treatments that affect the cytoskeleton. Here we demonstrate that direct mechanical stimulation (stretching) of an actin stress fiber using optical tweezers can activate MS channels in cultured human umbilical vein endothelial cells (HUVECs). Furthermore, by using high-speed total internal

reflection microscopy, we visualized spots of Ca²⁺ influx across individual MS channels distributed near focal adhesions in the basal surface of HUVECs. This study provides the first direct evidence that the cytoskeleton works as a force-transmitting and force-focusing molecular device to activate MS channels in eukaryotic cells.

Supplementary material available online at
<http://jcs.biologists.org/cgi/content/full/121/4/496/DC1>

Key words: Actin, Mechanosensitive channel, Mechanical stress, Stress fiber

Introduction

Mechanosensitive (MS) channels are expressed in a variety of cells (Sachs, 1991). They are thought to play crucial roles not only in the mechanosensation by specialized mechanosensors such as hair cells and baroreceptors, but also in volume regulation and locomotion in ordinary cells (Gillespie and Walker, 2001). Elucidation of the molecular and biophysical mechanisms involved in the regulation of MS channel activities is a central interest in basic biology. To date, two mechanisms have been proposed for MS channel activation. One is that tension development in the lipid bilayer directly activates MS channels. This is mostly based on biophysical analyses of the bacterial large conductance mechanosensitive channel MscL (Sukharev et al., 2001; Sukharev et al., 1994), and TRPC1 (Maroto et al., 2005) reconstituted in cytoskeleton-free liposomes. The second mechanism proposes that the extracellular matrix (Du et al., 1996) and cytoskeleton (Fukushige et al., 1999; Savage et al., 1989; Sokabe et al., 1991) are involved in channel activation; more specifically, that tension in the cytoskeleton activates MS channels. A couple of studies (Byfield et al., 2004; Evans and Waugh, 1977) have shown that a membrane interacting with cytoskeletons is stiffer than the membrane alone, implying that cytoskeletons would make the membrane a more efficient force-transmitting device. In fact, a certain MS channel shows a loss of mechanosensitivity when examined in a cytoskeleton-free membrane (Zhang et al., 2000). It has also been reported that the cytoskeleton by itself will work as a force-focusing structure (Hu et al., 2003) owing to its linear structure with a relatively high elastic modulus (Kojima et al., 1994). Unfortunately, however, this idea is based on indirect evidence from electrophysiological and genetic analyses in eukaryotic cells (Corey et al., 2004). It is imperative to design and conduct experiments in which one can directly manipulate the

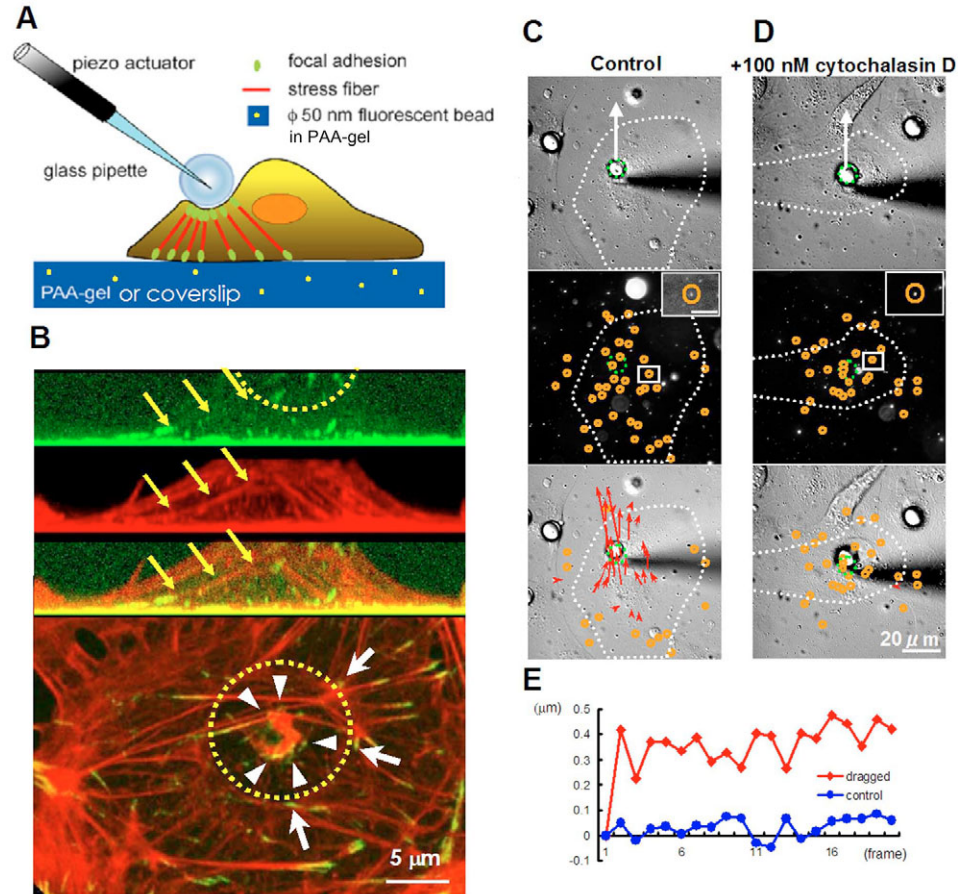
cytoskeleton while recording MS channel activities, preferably in intact cells.

We used intact cultured human umbilical vein endothelial cells (HUVECs) to demonstrate that MS channels are activated by stress in the cytoskeleton. When HUVECs are subjected to uniaxial stretch, MS channels are activated, followed by an increase in the intracellular Ca²⁺ concentration ([Ca²⁺]_i) because of Ca²⁺ influx through the channels (Naruse and Sokabe, 1993). Stretching the extracellular substrate generates stress in the actin cytoskeleton (Pourati et al., 1998), which has been postulated to activate MS channels. However, detailed electrophysiological and imaging analyses of the channel activation is technically very difficult with this type of mechanical stimulation because of the movement of the cells upon stretching. We used an assay system in which it is possible to apply localized mechanical stresses onto focal adhesions to activate MS channels by dragging fibronectin-conjugated beads adhering to the dorsal cell surface (Hu et al., 2003) or injecting phalloidin-conjugated beads into cells, which then bind to actin stress fibers (and/or actin filaments). We demonstrate that direct mechanical stimulation (stretching) of the actin cytoskeleton using optical tweezers can activate MS channels in cultured HUVECs.

Results

A new assay system was used that enables detailed measurement of increases in the [Ca²⁺]_i level while recording MS channel currents in cells subjected to localized mechanical stimuli. First, glass beads conjugated with fibronectin (FN) were plated on cultured HUVECs. The beads adhered to the apical cell surface within a few minutes (Fig. 1), followed by accumulation of β1 integrin, paxillin and vinculin molecules just beneath the beads over the next few minutes, resulting in the formation of focal

Fig. 1. Localized mechanical stimuli were applied to HUVECs by displacing an FN bead. (A) Schematic drawing of the experimental set-up. A HUVEC was plated on a fibronectin-conjugated elastic polyacrylamide gel substrate (blue). (B) HUVECs were stained with anti-paxillin antibodies (upper panel) and Rhodamine-phalloidin (middle panel), and sectioned in the x - z plane. These images are overlaid in the panel below. The yellow semi-circle shows the position of the FN bead. Stress fibers (yellow arrows) connect the apical focal adhesions (FAs) to the basal FAs. The bottom panel shows the x - y confocal image of the cell. A 10 μm bead promoted formation of focal adhesions on the apical surface (shown by white arrows). The pattern of FAs underneath the FN bead was scattered and irregular (arrowheads). FAs on the cell base were also imaged. Twenty confocal images (5 μm thickness) were projected to the x - y plane. (C) An example of gel deformation caused by a mechanical stimulation. An FN bead (shown by green dotted circle) on a HUVEC (white broken line denotes the cell perimeter) was displaced by a piezoelectric-driven glass pipette (shadows in the top and bottom panels). Small orange circles indicate the position of 50 nm fluorescent beads (middle panel). Insets show fluorescent beads at higher magnification (a fluorescent spot at the centre of the circle; scale bar, 5 μm). Each red arrow in the bottom panel indicates the direction and relative amplitude of fluorescent particle displacement (longest arrow corresponds to 0.76 μm displacement) when the FN bead was moved 4 μm in the direction shown in the top panel by an arrow. (D) Very small substratum deformation underneath the bead was observed in cytochalasin-D-treated cells (note red arrow in the lower right marginal region of the cell). (E) Time course of the displacement of a 50 nm bead exposed to the mechanical stimulus along with the time course of another bead that did not move because it is located far from the FN bead ($>40 \mu\text{m}$). The interval between frames was 1 second.



adhesions (FAs). These FAs were connected to the pre-existing FAs at the basal (or abluminal) cell surface via actin stress fibers within 30 minutes of plating (Fig. 1B). The pattern of FAs underneath the FN bead was somewhat different from the control; the staining patterns were scattered and irregular (Fig. 1B; arrowheads). Fig. 1B shows that 10 μm diameter glass beads promoted formation of focal adhesions on the apical surface. The size of FAs on the apical and basal surfaces was roughly the same. With this bead–apical–FA–stress-fiber–basal-FA linkage it is possible to apply mechanical forces to the basal FAs by displacing the bead with a piezoelectric-driven glass capillary.

Mechanical stimulation of basal FAs via stress fibers by FN bead displacement

To elucidate the targets of the force generated by FN bead displacement, we used a polyacrylamide (PAA) gel substrate culture system as described (Munevar et al., 2001). Considering the supramolecular complex under the FN bead (apical-FA–stress-fiber–basal-FA), one of the most probable targets should be the FAs at the basal cell surface. To test this hypothesis, HUVECs were cultured on fibronectin-conjugated polyacrylamide gel containing fluorescent particles (50 nm diameter), and time-lapse imaging of deformation of the gel was performed (Fig. 1A). The amplitude and direction of deformation in the gel upon displacement of a FN

bead by 4 μm were estimated as shown in Fig. 1C. Image analysis of movements of the fluorescent particles showed that the mechanical force was transmitted to an area approximately 20 μm from the bead position when it was projected to the basal cell surface, where the substrate was pulled in the direction of bead displacement (Fig. 1C). Fig. 1E shows the time course of the displacement of a 50 nm bead exposed to the mechanical stimulus. The force required for 1 μm displacement of the FN bead was estimated at $35.7 \pm 5 \text{ nN}$ ($n=5$).

When cells were pretreated with cytochalasin D (cytoD) (100 nM, 30 minutes, Fig. 1D), a similar degree of deformation of the apical cell surface by the FN-bead displacement was observed, but the force required for the same displacement of the bead on the cytoD-treated cells was estimated at only $2.3 \pm 0.5 \text{ nN}$ ($n=6$). These small numbers are probably due to the disassembly of mechanically resistive stress fibers by cytoD (supplementary material Fig. S1).

The shape and distribution of the basal FAs detected by reflection interference contrast microscopy did not change before or after mechanical stimulation in control and cytoD-treated cells when they were cultured on coverslips (data not shown), indicating that the FAs were not detached from the substrate by the stimulation. Therefore, all further experiments were carried out on cells cultured on coverslips.

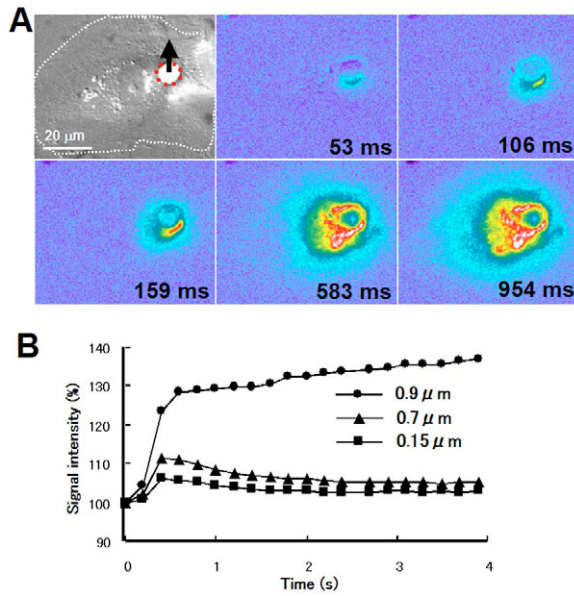


Fig. 2. Mechanical stimulation evoked a transient increase in $[Ca^{2+}]_i$ and induced whole-cell inward current. (A) Displacement of the FN bead ($1 \mu\text{m}$ for 100 milliseconds) evoked an increase in $[Ca^{2+}]_i$ within 53 milliseconds from the start of stimulation. The red circle in the DIC image denotes the FN bead and the white dotted line shows the perimeter of the HUVEC. The black arrow indicates the direction of displacement. (B) Increase in $[Ca^{2+}]_i$ with sequential displacement of the FN bead for 0.15, 0.7 and $0.9 \mu\text{m}$. Typical data are shown in the figure. The increase in the signal intensity by 0.5–0.7 μm displacement of FN beads was significantly larger than that of 0.15–0.2 μm displacement ($P < 0.05$; $n = 5$).

Local $[Ca^{2+}]_i$ increase via MS channels by FN-bead displacement

Immediately after the displacement of the FN bead, $[Ca^{2+}]_i$ increased rapidly and spread over the cell in a few seconds (Fig. 2A), returned to the resting $[Ca^{2+}]_i$ level in 3 minutes. The amplitude of the $[Ca^{2+}]_i$ increase increased monotonically with the degree of displacement (0.15–0.9 μm ; a typical example of the response is shown in Fig. 2B); the response was nonlinear to the amplitude of the FN-bead displacement. The minimal response was induced by 0.15 μm ($0.34 \pm 0.06 \mu\text{m}$, mean \pm s.e.m., $n = 8$) displacement.

The transient increase in $[Ca^{2+}]_i$ was largely inhibited ($88.1 \pm 4.3\%$, $n = 5$) by $20 \mu\text{M}$ Gd^{3+} or in Ca^{2+} -free medium (supplementary material Fig. S2), but was not affected by thapsigargin ($1 \mu\text{M}$), suggesting that the $[Ca^{2+}]_i$ increase was mediated by the influx of Ca^{2+} through MS channels.

We examined whether cytoskeletal structures were involved in the activation of the MS channels by FN-bead displacement. The FN-bead-dependent $[Ca^{2+}]_i$ increase was nearly perfectly abolished ($95.1 \pm 5.5\%$, $n = 3$, supplementary material Fig. S2) when cells were pretreated with the F-actin-disrupting agent cytoD (100 nM , 30 minutes). By contrast, the $[Ca^{2+}]_i$ increase was not affected by the microtubule-disrupting agent colcemid ($1 \mu\text{M}$, 30 minutes) when FN beads were displaced, suggesting that actin stress fibers are essential to induce the $[Ca^{2+}]_i$ increase caused by FN-bead displacement. There remains a question, however, whether the deformation of the submembranous actin network associated with membrane deformation contributes to the $[Ca^{2+}]_i$ increase. To address this we performed an alternative experiment in cytoD-untreated cells with an attached glass bead

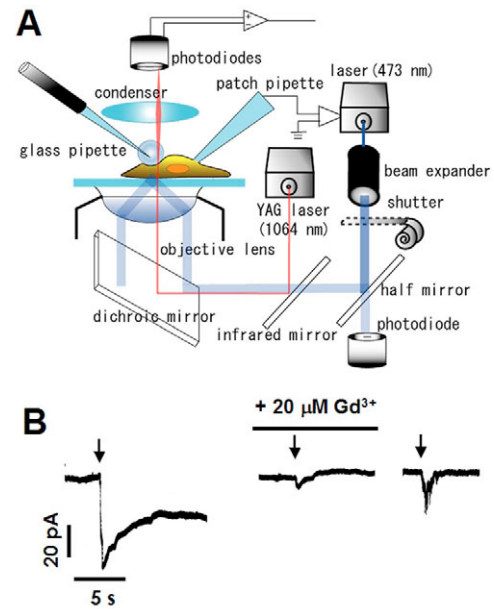


Fig. 3. Experimental set-up for patch-clamp recordings and high-speed TIRF microscopy, and inward currents induced by mechanical stimuli. (A) A whole-cell patch-clamp recording was made from a cell subjected to localized mechanical stimulation. The displacement of the FN bead was monitored with photodiodes during the experiment using an IR YAG laser. Blue laser light (473 nm) was introduced into the objective lens to produce an evanescent illumination for the measurement of $[Ca^{2+}]_i$ and was controlled with a high-speed shutter (results are shown in Fig. 5B). (B) Displacement of the bead induced an inward current. $20 \mu\text{M}$ Gd^{3+} reduced the amplitude of the inward current. The inward current partially recovered after the removal of Gd^{3+} (right trace). Arrows denote the displacement of the FN bead.

on the apical surface without FAs and linked the stress fibers underneath the bead. For this purpose, we prepared glass beads conjugated with IgG-anti-LDL receptor or IgG-non-stimulating anti- $\beta 1$ integrin (K-20), which did not induce formation of focal complexes or actin stress fibers underneath the bead when adhering to the dorsal cell surface. With these configurations, the same amplitude of bead displacement, which induced a comparable degree of deformation of the apical surface of the cell as the FN bead, did not evoke a $[Ca^{2+}]_i$ increase (supplementary material Fig. S2). We cannot completely exclude the possibility that a cytoD-sensitive network of actin filaments in the cell cortex that interacts mechanically with the adhered bead may play a role in mediating the activation of the MS channels. However, the above result showing that dragging an antibody-coated bead attached to the surface of control cells with the submembranous actin network intact did not induce a $[Ca^{2+}]_i$ increase, strongly suggests that the major force-transmitting device is the actin stress fiber.

Electrophysiology should provide a better means than Ca^{2+} imaging to make quantitative analyses of the MS channel properties. For this purpose we built the fully electronically controlled set-up shown in Fig. 3A, and made whole-cell patch-clamp recordings (Fig. 3A) to monitor mechanically induced channel currents. FN-bead displacement induced an inward current ($23.4 \pm 4 \text{ pA}$, $n = 15$) in less than 10 milliseconds and the current peaked within 100 milliseconds (Fig. 3B) then gradually declined. This transient inward current was also significantly reduced by $20 \mu\text{M}$ Gd^{3+} ($91.5 \pm 3.1\%$ inhibition, $n = 4$, Fig. 3B) as in the $[Ca^{2+}]_i$

transient response, suggesting that they are from the same origin – MS channels.

Direct mechanical stimulation of actin stress fibers activates MS channels

We developed a new experimental technique to test more directly the hypothesis that mechanical stress in the actin cytoskeleton can activate MS channels. Cells were microinjected with phalloidin-conjugated beads through a glass micropipette. The injected beads and actin stress fibers in fixed preparations were imaged by confocal microscopy (Fig. 4B), showing that most of the beads (or aggregates of beads) and stress fibers were overlapped in the same optical slice. In addition, live imaging of the preparation demonstrated that the beads stayed in the same position, suggesting that the beads were closely associated with stress fibers and/or actin networks that connect stress fibers. Although the resolution of the optics was not sufficient to conclude that the beads were bound to the stress fibers or actin networks, MS channel activation could only be elicited by dragging the phalloidin-conjugated beads (Fig. 4C) not by dragging control beads. This strongly suggests that the phalloidin-conjugated beads adhered to the actin cytoskeleton tightly enough to generate tension in the actin cytoskeleton and activate MS channels whether the bead adhered to actin cytoskeleton directly or indirectly.

A traction force to actin cytoskeleton was applied by dragging a bead aggregate (approximately 400 nm in diameter) with laser tweezers. MS channel currents were recorded with the whole-cell patch clamp technique while monitoring the position of the trapping point of laser tweezers (Fig. 4A). When the trapping point passed the aggregate, a transient inward current was evoked (Fig. 4C) and returned to a basal level in less than 1 second. For a second stimulation, the direction of the movement of trapping point was reversed and passed the same aggregate, which again evoked an inward current with a similar amplitude (Fig. 4C, right arrow). The average amplitude of the inward current was 7.4 ± 1.1 pA ($n=22$), which was 32% of that induced by FN-bead displacement. The amplitude of the force of the laser trapping was estimated at 5.5 pN (see Materials and Methods). When the laser-trapping focus passed an aggregate of phalloidin-conjugated beads, the $[Ca^{2+}]_i$ increased (Fig. 4D), showing that the Ca^{2+} -permeable MS channels are activated by direct manipulation of actin cytoskeleton. When a non-labeled bead was trapped and moved by the optical tweezers, force was transmitted to the substrate in a similar way without activating MS channels; these beads were displaced slightly and were probably stopped by their interaction with subcellular structures, such as microtubules, intermediate filaments or internal membranes. The stress in these structures was not transmitted to the MS channels or perhaps was not large enough to activate them.

MS channels locate in the vicinity of FAs: verification by imaging the sites of Ca^{2+} influx through individual channels

The above results showing that MS channels are activated by the stress in actin stress fibers terminated at basal FAs leads to the hypothesis that MS channels in HUVECs locate near FAs. To test this idea we examined the hypothetical colocalization of MS channels and FAs by imaging the $[Ca^{2+}]_i$ microdomain that comprise high- $[Ca^{2+}]_i$ regions at the cytoplasmic vestibule of Ca^{2+} -permeable channels (Zenisek et al., 2003; Zou et al., 2002). We imaged $[Ca^{2+}]_i$ microdomains using high-speed evanescent-field microscopy (Fig. 5A), while monitoring the distribution of FAs by reflection interference contrast microscopy (Fig. 5Ab). The earliest

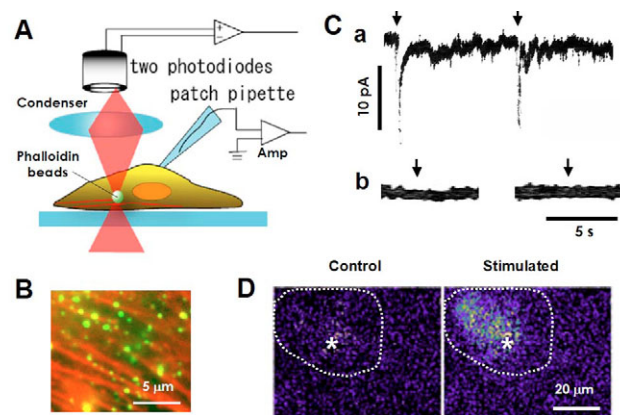


Fig. 4. Activation of MS channels by applying mechanical force to beads attached to actin stress fibers. (A) Phalloidin-conjugated 40 nm fluorescent beads were microinjected into HUVECs. These beads bound to the actin stress fibers and were trapped by laser optical tweezers. The movement of the trapping point was monitored with two photodiodes. Whole-cell patch-clamp recordings were made from the same cell. (B) Phalloidin-conjugated green fluorescent beads were located along the actin stress fibers (red). The cell was fixed 30 minutes after microinjection and stained with Rhodamine-phalloidin in this case. (C) A transient inward current was induced when the optical tweezers transiently passed an aggregate of phalloidin coated beads (shown by the two arrows in a). No current was induced when the same experiment was made with control beads (b). (D) The same mechanical stimulation with optical tweezers increased the $[Ca^{2+}]_i$. The asterisks in the indicate the site of the aggregate of phalloidin-conjugated beads. The white broken line shows an outline of the HUVEC.

Ca^{2+} image (Fig. 5Ad) taken at 17 milliseconds after the onset of mechanical stimulation by a FN-bead displacement was superimposed over the FA image, as shown in Fig. 5Ah, and examined the relationship between the localization of the $[Ca^{2+}]_i$ microdomain and that of FAs. As indicated by the two arrowheads in Fig. 5Ah, the high $[Ca^{2+}]_i$ region coincides with FAs, suggesting that MS channels are located near (or at) FAs. To confirm that the observed $[Ca^{2+}]_i$ regions arose from the Ca^{2+} influx across the basal cell surface, we performed high-speed line-scan confocal imaging of $[Ca^{2+}]_i$, in which Ca^{2+} entered across both the top and bottom membranes (<4.3 milliseconds). Ca^{2+} started to increase in concentration at the middle of the cell approximately 13 milliseconds after mechanical stimulation (supplementary material Fig. S3). Therefore, the larger high- $[Ca^{2+}]_i$ region in Fig. 5 under the bead at 17 milliseconds should be dominated by the Ca^{2+} influx from the bottom membrane of the cell. In addition, as the Ca^{2+} influx from the dorsal surface was only observed just underneath the bead, the small high- $[Ca^{2+}]_i$ increase approximately 10 μ m away from the bead shown at the lower right in Fig. 5Ah reflects the Ca^{2+} influx from the bottom surface. However, the resolution of the image of the high- $[Ca^{2+}]_i$ regions taken by this method was not high enough to visualize the exact locus of $[Ca^{2+}]_i$ microdomains owing to the relatively fast diffusion of Ca^{2+} after entry into the cytoplasm.

In order to visualize the locus of the $[Ca^{2+}]_i$ microdomains more precisely, it is necessary to acquire a much faster snapshot (\sim milliseconds) of the $[Ca^{2+}]_i$ increase immediately after the onset of mechanical stimulation. We imaged the distribution of $\beta 1$ integrin in living HUVECs, as previously described (Kawakami et al., 2001), to characterize the distribution of $[Ca^{2+}]_i$ increases. The integrin in live images colocalized with paxillin, confirming that

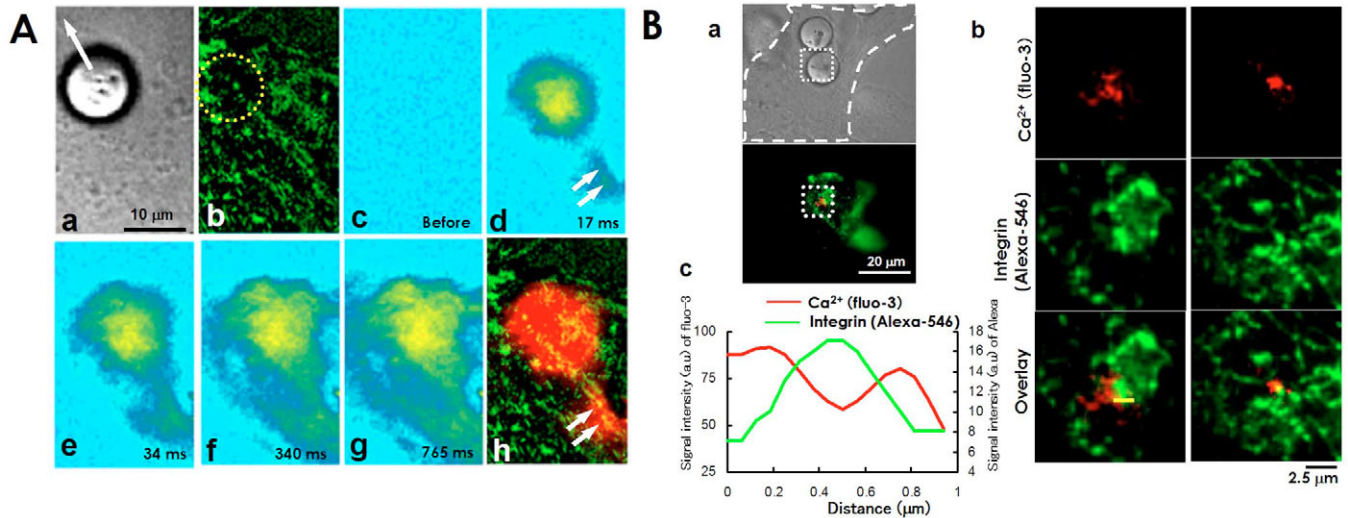


Fig. 5. Activation of MS channels in the vicinity of FAs by mechanical stimulation. Time-lapse imaging of the increase in $[Ca^{2+}]_i$ at a time resolution of 17 milliseconds (A) and a 2 millisecond snapshot image of the $[Ca^{2+}]_i$ increase (B). (A) The FN bead was displaced by $1\ \mu\text{m}$ in the direction indicated by the arrow (a). The distribution of FAs was imaged by interference reflection contrast microscopy; green spots denote the FAs (b). (c–g) A series of time-lapse images of the increase in $[Ca^{2+}]_i$ caused by the mechanical stimulation. (h) Superimposed images of b and d (green, FAs; red, $[Ca^{2+}]_i$ increase). The white arrows indicate FAs inside of the area of the $[Ca^{2+}]_i$ increase. (B) DIC (a, upper) and TIRF (a, lower) images of a cell at low magnification. The area enclosed by the white dotted rectangle in a is magnified in b. Regions of high $[Ca^{2+}]_i$ ($[Ca^{2+}]_i$ microdomains) 2–4 milliseconds after the onset of the stimulation are shown as red spots. These spots are located in the vicinity of integrin clusters (green). The upper left panel in b shows approximately 10 $[Ca^{2+}]_i$ microdomains. The middle left panel shows $\beta 1$ integrin and the lower left panel shows an overlay of the $[Ca^{2+}]_i$ microdomain and the integrin. The right-hand panels in b show another example of the $[Ca^{2+}]_i$ microdomains 0–2 milliseconds after the onset of the stimulation. The graph in c shows the intensity profiles of fluo-3 and anti- $\beta 1$ -integrin fluorescence in the region denoted by the yellow line in the lower left panel in b.

the integrin clusters were FAs (supplementary material Fig. S4). In this experiment, $[Ca^{2+}]_i$ transients under the bead were imaged with a single brief (2 millisecond duration) evanescent laser light illumination at, or 2 milliseconds after, the onset of mechanical stimulation (Fig. 5B-b). A mean of 4 ± 0.94 (\pm s.e.m.; $n=8$) $[Ca^{2+}]_i$ microdomains appeared in the vicinity of FAs underneath the FN bead with 2 milliseconds of illumination; the diameter of the microdomain was $0.96 \pm 0.07\ \mu\text{m}$ ($n=33$), which agrees with the value in a previous report (Zou et al., 2002) and also theoretical estimations (discussed later). The number of $[Ca^{2+}]_i$ microdomains also principally agrees with the number of MS channels estimated from our whole-cell current measurements as follows. The peak amplitude of the whole-cell MS current (23 pA at a holding potential of -40 mV) evoked by displacing a FN bead corresponds to 14–24 MS channels, given that the conductance of a single MS channel in HUVECs ranges from 24 to 40 pS (Lansman et al., 1987; Popp et al., 1992; Yao et al., 2001). If half of them were located on the basal surface of the cell, we would expect to see seven to twelve channels (or microdomains) under these recording conditions. This is roughly consistent with the above observation. All these results support the idea that the $[Ca^{2+}]_i$ microdomain in this study represents a single activated MS channel or a single cluster of a few MS channels. Interestingly, the center of individual $[Ca^{2+}]_i$ microdomains did not overlap with FAs in all 27 $[Ca^{2+}]_i$ microdomains examined; but rather lay 760 ± 60 nm (mean \pm s.e.m.; $n=27$) from the center of FAs (Fig. 5B); the area of integrin clusters did not overlap that of $[Ca^{2+}]_i$ microdomains in all cases examined. These results suggest that MS channels in the vicinity of FAs were activated by the force exerted along certain structures, possibly the bilayer and/or submembranous cytoskeletons, which may link MS channels with the FAs.

Discussion

The importance of the cytoskeleton for activating MS channels has repeatedly been suggested based on electrophysiological analyses of single MS channel activities (Sachs, 1991; Sokabe et al., 1991; Sukharev et al., 1999; Yao et al., 2001). However, evidence from the studies on cytoskeleton involvement in cell mechanotransduction is still indirect. The present study has succeeded in demonstrating by a combination of electrophysiological, advanced imaging and laser trapping techniques that stress in the actin cytoskeleton can activate MS channels in eukaryotic cells. There follows the question of the extent to which the cytoskeleton contributes to the MS channel activation in eukaryotic cells.

In HUVECs, the force generated by the laser trapping (5.5 pN) was most likely transmitted through an actin filament to MS channels, where it activated them. The resulting inward current was ~ 7.4 pA at -40 mV, which corresponds to an activation of five to eight MS channels (assuming the single channel conductance of 24–40 pS). This suggests that a sub-pN force could activate a single MS channel in an intact cell. It should be noted that although there are a large number of channels within a cell, only a very limited number of channels (5–8 in the above case) were activated by the stimulus. In addition, because of the transient nature of the trapping, the measured currents might not reflect the full activation level and the number of activated MS channels may be underestimated, while the force for channel activation is overestimated. We speculate that this relatively small force works on the MS channels (and their accessory proteins), which have the machinery to open the channel under such small forces. Compared with activation forces in MscL (Sukharev et al., 1999; Gullingsrud and Schulten, 2003), where approximately 40 pN was used in MD

simulations, those in the HUVEC MS channel seem to be much smaller, suggesting that cytoskeletal structures work as an efficient force-transmitting and -focusing structure to confer higher mechanosensitivity on the MS channel in eukaryotic cells.

The force applied to the cell surface by the FN bead (35 nN) induced an inward current of 23 pA, whereas the optical manipulation (5.5 pN) of the actin cytoskeleton induced an inward current of 7.4 pA. These results suggest that a very small fraction of the force applied to the cell surface was still sufficient to activate MS channels; most of the force on the FAs (or integrins) would be transmitted to the extracellular substrate via the cytoskeleton, organelles and FAs. The specific molecular components that transmit the force from an actin stress fiber to the MS channels presumably form a structural linkage, but they are not identified here, and remain an area for future study.

We imaged Ca^{2+} influx through a channel or a cluster of channels as a Ca^{2+} spot (microdomain). A recent study demonstrated that a Ca^{2+} microdomain reflects the activation of a single MS channel (Zou et al., 2002). The diameter of the Ca^{2+} microdomain (2.2 μm , 15 milliseconds after channel opening) is similar to that imaged in this study, supporting the idea that it is possible to image the activation of a single MS channel or a small number of MS channels in a cluster. The theoretical estimation of the size of a Ca^{2+} microdomain also supports the above idea. Using the diffusion constant of Ca^{2+} in cytoplasm [0.6×10^{-6} $\text{cm}^2/\text{second}$ (Hodgkin and Keynes, 1957)], the diameter of the Ca^{2+} microdomain 4 milliseconds after the opening of a Ca^{2+} channel is calculated to be 1.1 μm , a value close to that (0.96 μm) obtained in this study. Whole-cell electrical recording corresponds not only to the Ca^{2+} influx in, or near, FAs, but also to other channels on distant sites on the surface membrane. These channels might be activated by forces exerted, for example, on glass beads bound to cytoskeleton through integrins, or on nanobeads directly bound to actin fibers (Fig. 5Ad). The mechanical-stimuli-induced [Ca^{2+}]_i increase in the apical and basal areas and the [Ca^{2+}]_i imaging 4.3 milliseconds from the stimulus onset (supplementary material Fig. S3) showed that [Ca^{2+}]_i increases at apical and basal areas were roughly the same, suggesting that MS channels in the apical and basal membranes are activated to a similar degree just after the stimulus onset. [Ca^{2+}]_i microdomains could only be observed underneath the FN bead by TIRFM just after the stimulus onset. Therefore, the initial part of the current less than 4 milliseconds from the onset of the mechanical stimuli could correspond to the [Ca^{2+}]_i microdomains. Therefore, approximately half of the current may be accounted for by these [Ca^{2+}]_i microdomains.

The present study not only provides direct evidence that development of tension in actin stress fibers can activate MS channels in intact cells, but also reveals a new function of the actin cytoskeleton as a force-transmitting and -focusing device between integrins and MS channels. Such a concept has already been suggested in previous studies (Doyle and Lee, 2005; Hu et al., 2003; Munevar et al., 2004). Taken together, these studies along with ours open the door to a complex but intriguing world of cellular mechanotransduction involving remote activation and regulation of MS channels, since stress in the actin cytoskeleton changes during a variety of mechano-related cell behavior, such as morphogenesis and locomotion. A good example can be seen in the locomotion of keratocytes (Doyle and Lee, 2005), in which increased traction stresses induce a Gd^{3+} -sensitive [Ca^{2+}]_i transient change, resulting in adhesion disassembly and rapid retraction at

the rear of the cell. It is suggested that stress in the actin cytoskeleton will be focused on the MS channel to induce its activation and following this, Gd^{3+} -sensitive Ca^{2+} entry. The relationship between MS channels and cell adhesion has also been discussed in a recent report (Doyle and Lee, 2005). A range of cell behaviors, including cell migration (Doyle and Lee, 2005; Munevar et al., 2004; Tanaka et al., 2005) and morphogenesis (Naruse et al., 1998) are inhibited by the potential MS channel blocker Gd^{3+} . Stretching forces applied through flexible substrata also induced increases in both intracellular Ca^{2+} concentration and traction forces of NIH3T3 fibroblasts (Munevar et al., 2004). They suggest that stretch-activated Ca^{2+} entry in the frontal region regulates the organization of focal adhesions and the output of mechanical forces. The mechanotransduction mechanism proposed in this study, effected by a molecular complex of the MS channel, the cytoskeleton and cell adhesion, evidently play an important role in these cellular functions.

Materials and Methods

Cell preparation

Endothelial cells were prepared from a human umbilical cord vein as described previously (Gimbrone and Fareed, 1976; Kawakami et al., 2001). HUVECs were transferred into a handmade chamber for TIRF microscopy and incubated with an Alexa Fluor 488- or Alexa Fluor 546-labeled monoclonal antibody against $\beta 1$ integrin (anti-CD29, Endogen) for 30–45 minutes; details of the procedure for immunofluorescent staining of integrins in living HUVECs are provided in our previous report (Kawakami et al., 2001).

Preparation of glass beads conjugated with fibronectin or antibody

Glass beads (10 μm diameter, Duke Scientific) were conjugated with fibronectin (FN) or anti-mouse IgG respectively, as described previously (Jacobson et al., 1978). FN-conjugated beads were stored at -20°C in PBS containing 50% glycerol, and washed with culture medium before use. Goat IgG anti-mouse IgG-conjugated glass beads were treated with 10 $\mu\text{g}/\text{ml}$ of non-stimulating anti- $\beta 1$ integrin mouse monoclonal IgG (K-20, ICN) or anti-LDL receptor mouse monoclonal IgG (Calbiochem) for 30 minutes and washed twice in PBS before use.

Force application

A FN-coated bead was displaced by a piezoelectric-driven glass pipette (approximately 1 μm) for 100 milliseconds. The pipette was made from a glass capillary (1 mm diameter, Narishige, Japan) with a programmable puller (Model P-97, Sutter Instrument Co.), and the tip was fire polished. The mechanical force required to displace the FN bead by 1 μm was 35.7 ± 5.0 nN in five cells. The force applied to the bead was estimated as follows. First, the force-bending relation at the tip of the glass capillary was determined using the calibrated tip of an AFM probe (SN-AF01, Olympus, Japan), yielding a linear relationship. Then, the relationship between the bending of the capillary tip and displacement of a FN-bead was monitored with a CCD camera. The bending of the capillary was monitored when an FN bead was displaced 1 μm , and the force applied to the FN bead was estimated. The extent of the deformation of the surface of a cell by the FN bead and control bead displacement was monitored with DIC microscopy and/or confocal microscopy. Confocal imaging also revealed that the fibronectin-coated beads of 10 μm diameter remained on the dorsal cell surface and were not ingested during the entire experimental period, which was usually less than 1 hour after plating of the beads.

Polyacrylamide gel substrate culture

The polyacrylamide gel substrate was prepared as reported (Munevar et al., 2001) with minor modifications. Fluorescent beads (Fluoresbrite 50 nm diameter, Polyscience) in 1 μl solution were precipitated in a microcentrifuge (CF 15R, Hitachi, Tokyo, Japan) at 15,000 rpm, and then the precipitate was resuspended in 300 μl polyacrylamide gel solution (10% acrylamide/0.25% bis-acrylamide). 20 μl polyacrylamide gel solution was placed in a culture chamber and covered with a 15 mm diameter coverslip. The surface of the PAA gel was conjugated with fibronectin (100 $\mu\text{g}/\text{ml}$) as described (Munevar et al., 2001). Time-lapse images of the fluorescent beads underneath (within a few μm) the cells were recorded during force application. Movements of the fluorescent beads were analyzed with a particle-tracking program (MetaMorph, Universal Imaging). Polyacrylamide substrates were used only for Fig. 1.

Measurement of intracellular Ca^{2+} concentration

Changes in the intracellular concentration of Ca^{2+} were estimated with fluo-3AM (Dojindo, Kumamoto, Japan). Fluo-3 was excited with light (480 nm) from a xenon

lamp (LAMBDA DG-4, Sutter Instruments) or a solid phase laser (473 nm, Solid State 473, HK5510, Shimadzu, Kyoto, Japan). Images were obtained with a cooled-CCD camera (Coolsnap/fx, Roper Scientific) after fluorescence had passed through a 510-nm long wave path filter. The number of $[Ca^{2+}]_i$ microdomains in the basal cell surface was counted as follows. First, a $[Ca^{2+}]_i$ image after a stimulation was divided by the pre-stimulation image to obtain a normalized image. The peak intensity of the normalized image was measured after subtracting the background level. Two thirds of the peak value was used as a threshold to isolate the $[Ca^{2+}]_i$ microdomains. Fluorescence spots larger than 0.4 μm were counted as $[Ca^{2+}]_i$ microdomains. The peak intensity of integrin fluorescence image was measured after subtracting the background level, and two thirds of the peak value was used as a threshold to isolate integrin clusters.

A multi-mode microscope capable of TIRF, DIC, EpiF and RIC imaging

TIRF optics were incorporated into an inverted microscope (TE300, Nikon) equipped with optics for differential interference contrast (DIC), epifluorescence and reflection interference contrast microscopy as described previously (Kawakami et al., 2001). A CLSF microscope (LSM510, Zeiss) was used to analyze the three dimensional distribution of the integrins and actin stress fibers and to perform line scan imaging. The chamber for the TIRF imaging consists of a high index cover glass (optical index 1.78, Olympus) and a small chamber made of silicone plate. A laser beam (473 nm, 18 mW, Solid State 473, HK5510, Shimadzu; or 532 nm, 50 mW, DPSS532, Coherent) was attenuated and directed into the objective lens ($\times 100$, NA 1.65, Olympus) to generate evanescent light at the surface of the high index coverslip (Fig. 3A). TIRF images were focused on the cooled-CCD camera. The images obtained were processed with MetaMorph (Universal Imaging). The size of the $[Ca^{2+}]_i$ microdomain was estimated as follows; first the peak intensity of the fluorescence of each microdomain was measured and the threshold was set at two-thirds of each peak intensity to isolate the microdomain from the background fluorescence, the microdomain appeared an island of fluorescence in the sea after removing the background fluorescence, and the diameter of the island was measured. This procedure was applied for all microdomains. The temperature of the chamber was maintained at approximately 37°C.

Microinjection of fluorescent beads

Streptavidin-coated fluorescent beads (100 μl) (Molecular Probes) were incubated with 50 U/ml of Biotin phalloidin (Molecular Probes) in PBS overnight at 4°C, and were centrifuged by microcentrifuge (CF 15R, Hitachi) at 15,000 rpm for 10 minutes. The beads were resuspended in the microinjection buffer (100 mM KCl and 10 mM HEPES-KOH, pH 7.4), filtered through a Millipore filter (Ultraclean, pore size 0.22 μm), and introduced into HUVECs by a microinjection method as described (Hiramoto, 1974). We performed experiments 3 hours after the injection of the intracellular solution (100 mM KCl and 10 mM HEPES, pH 7.4) with beads into the cell, and did not see any significant changes in the structure of the cell during the experiment, which was confirmed by videomicroscopy.

Optical trapping of beads attached to stress fibers

The optical trapping system was based on a previous report (Ashkin et al., 1987). A polarized beam from a near-infrared (1064 nm) YAG laser (model DPY321, Coherent, Dieburg, Germany) was passed through a $\times 7$ beam expander (Melles Griot, Japan), and iris transfer unit (Sigma Koki, Tokyo, Japan), and focused on the phalloidin-conjugated beads through an objective lens (NA. 1.65, $\times 100$, Olympus). A remote beam steering system (Sigma Koki) was introduced to steer the laser trapping point. The maximum retention force of the 1064 nm laser (32 mW) was calibrated using the viscous dragging method (Tatsumi and Katayama, 1999). When a bead (1.0 μm diameter, Polyscience) was trapped, the mean retention force was estimated at 56.7 pN, and the retention force of trapping a 0.4 μm bead was estimated at 5.5 ± 0.45 pN (mean \pm s.d., $n=5$), and that of trapping an aggregate (approximately 0.4 μm) of 40 nm beads (Molecular Probes, USA) was almost in the same range. Optical trapping did not induce any injury current when the laser light was focused on a cell. Before the dragging of the aggregate, the focus of the tweezers was placed more than 2 μm away from the aggregate to avoid possible mechanical stimulation. Then it was moved toward the aggregate at 10 $\mu\text{m}/\text{second}$.

High-speed image acquisition

The experimental set-up for high-speed imaging of $[Ca^{2+}]_i$ is shown in Fig. 3A. Mechanical stimulation by the piezoelectric-driven glass pipette, evanescent illumination and image acquisition by the CCD camera are electrically controlled with MetaMorph (Universal Imaging). A 2 millisecond laser illumination was carried out using a camera equipped with a high-speed shutter (α sweet, Minolta). The displacement of the FN bead by the piezoelectric-driven glass pipette was monitored by projecting the image of the bead onto two photodiodes placed above the bead.

Patch-clamp recording

HUVECs were voltage clamped using the whole-cell patch-clamp technique with a patch-clamp amplifier (Axopatch 200A, Axon Instruments, Union City, CA). Patch electrodes were made from glass capillaries (Harvard Apparatus, Kent, UK) by a

vertical electrode puller (PP-83, Narishige, Tokyo, Japan) and heat polished with a microforge (MF-83, Narishige). The resistance of the pipette was 3–8 M Ω . Membrane currents were filtered using a four-pole Bessel filter (5 kHz) and recorded on a chart or analyzed by software (pCLAMP 5, Axon Instruments). All experiments were conducted at room temperature. The ionic composition of the pipette solution was: 70 mM KCl, 4 mM NaCl, 1 mM MgCl₂, 85 mM sucrose, 10 mM HEPES, 5 mM EGTA and solution was adjusted to pH 7.2 with KOH.

We thank D. T. Kiyoshima for technical assistance. This work was supported in part by Grants-in-aid for General Scientific Research (13480216 to M.S. and 14580769 to H.T.), Scientific Research on Priority Areas (15086270 to M.S.), Creative Research (16GS0308 to M.S.) from the Ministry of Education Science Sports and Culture and a grant from Japan Space Forum (to M.S. and H.T.).

References

- Ashkin, A., Dziedzic, J. M. and Yamane, T. (1987). Optical trapping and manipulation of single cells using infrared laser beams. *Nature* **330**, 769–771.
- Byfield, F. J., Aranda-Espinoza, H., Romanenko, V. G., Rothblat, G. H. and Levitan, I. (2004). Cholesterol depletion increases membrane stiffness of aortic endothelial cells. *Biophys. J.* **87**, 3336–3343.
- Corey, D. P., Garcia-Anoveros, J., Holt, J. R., Kwan, K. Y., Lin, S. Y., Vollrath, M. A., Amalfitano, A., Cheung, E. L., Derfler, B. H., Duggan, A. et al. (2004). TRPA1 is a candidate for the mechanosensitive transduction channel of vertebrate hair cells. *Nature* **432**, 723–730.
- Doyle, A. D. and Lee, J. (2005). Cyclic changes in keratocyte speed and traction stress arise from Ca^{2+} -dependent regulation of cell adhesiveness. *J. Cell Sci.* **118**, 369–379.
- Du, H., Gu, G., William, C. M. and Chalfie, M. (1996). Extracellular proteins needed for *C. elegans* mechanosensation. *Neuron* **16**, 183–194.
- Evans, E. A. and Waugh, R. (1977). Osmotic correction to elastic area compressibility measurements on red cell membrane. *Biophys. J.* **20**, 307–313.
- Fukushige, T., Siddiqui, Z. K., Chou, M., Culotti, J. G., Gogonea, C. B., Siddiqui, S. S. and Hamelin, M. (1999). MEC-12, an alpha-tubulin required for touch sensitivity in *C. elegans*. *J. Cell Sci.* **112**, 395–403.
- Gillespie, P. G. and Walker, R. G. (2001). Molecular basis of mechanosensory transduction. *Nature* **413**, 194–202.
- Gimbrone, M. A., Jr and Fareed, G. C. (1976). Transformation of cultured human vascular endothelium by SV40 DNA. *Cell* **9**, 685–693.
- Gullingsrud, J. and Schulten, K. (2003). Gating of MscL studied by steered molecular dynamics. *Biophys. J.* **85**, 2087–2099.
- Hiramoto, Y. (1974). A method of microinjection. *Exp. Cell Res.* **87**, 403–406.
- Hodgkin, A. L. and Keynes, R. D. (1957). Movement of labelled calcium in squid giant axons. *J. Physiol.* **138**, 253–281.
- Hu, S., Chen, J., Fabry, B., Numaguchi, Y., Gouldstone, A., Ingber, D. E., Fredberg, J. J., Butler, J. P. and Wang, N. (2003). Intracellular stress tomography reveals stress focusing and structural anisotropy in cytoskeleton of living cells. *Am. J. Physiol. Cell Physiol.* **285**, C1082–C1090.
- Jacobson, B. S., Cronin, J. and Branton, D. (1978). Coupling polylysine to glass beads for plasma membrane isolation. *Biochim. Biophys. Acta* **506**, 81–96.
- Kawakami, K., Tatsumi, H. and Sokabe, M. (2001). Dynamics of integrin clustering at focal contacts of endothelial cells studied by multimode imaging microscopy. *J. Cell Sci.* **114**, 3125–3135.
- Kojima, H., Ishijima, A. and Yanagida, T. (1994). Direct measurement of stiffness of single actin filaments with and without tropomyosin by in vitro nanomanipulation. *Proc. Natl. Acad. Sci. USA* **91**, 12962–12966.
- Lansman, J. B., Hallam, T. J. and Rink, T. J. (1987). Single stretch-activated ion channels in vascular endothelial cells as mechanotransducers? *Nature* **325**, 811–813.
- Maroto, R., Raso, A., Wood, T., Kurosky, A., Martinac, B. and Hamill, O. (2005). TRPC1 forms the stretch-activated cation channel in vertebrate cells. *Nat. Cell Biol.* **7**, 179–185.
- Munevar, S., Wang, Y.-L. and Dembo, M. (2001). Traction force microscopy of migrating normal and H-ras transformed 3T3 fibroblasts. *Biophys. J.* **80**, 1744–1757.
- Munevar, S., Wang, Y.-L. and Dembo, M. (2004). Regulation of mechanical interactions between fibroblasts and the substratum by stretch-activated Ca^{2+} entry. *J. Cell Sci.* **117**, 85–92.
- Naruse, K. and Sokabe, M. (1993). Involvement of stretch-activated ion channels in Ca^{2+} mobilization to mechanical stretch in endothelial cells. *Am. J. Physiol.* **264**, C1037–C1044.
- Naruse, K., Yamada, T. and Sokabe, M. (1998). Involvement of SA channels in orienting response of cultured endothelial cells to cyclic stretch. *Am. J. Physiol.* **274**, H1532–H1538.
- Popp, R., Hoyer, J., Meyer, J., Galla, H. J. and Gogolein, H. (1992). Stretch-activated non-selective cation channels in the antiluminal membrane of porcine cerebral capillaries. *J. Physiol.* **454**, 435–449.
- Pourati, J., Maniotis, A., Spiegel, D., Schaffer, J. L., Butler, J. P., Fredberg, J. J., Ingber, D. E., Stamenovic, D. and Wang, N. (1998). Is cytoskeletal tension a major determinant of cell deformability in adherent endothelial cells? *Am. J. Physiol.* **274**, C1283–C1289.
- Sachs, F. (1991). Mechanical transduction by membrane ion channels: a mini review. *Mol. Cell. Biochem.* **104**, 57–60.

- Savage, C., Hamelin, M., Culotti, J. G., Coulson, A., Albertson, D. G. and Chalfie, M. (1989). *mec-7* is a beta-tubulin gene required for the production of 15-protofilament microtubules in *Caenorhabditis elegans*. *Genes Dev.* **3**, 870-881.
- Sokabe, M., Sachs, F. and Jing, Z. Q. (1991). Quantitative video microscopy of patch clamped membranes stress, strain, capacitance, and stretch channel activation. *Biophys. J.* **59**, 722-728.
- Sukharev, S. I., Blount, P., Martinac, B., Blattner, F. R. and Kung, C. (1994). A large-conductance mechanosensitive channel in *E. coli* encoded by *mscL* alone. *Nature* **368**, 265-268.
- Sukharev, S. I., Sigurdson, W. J., Kung, C. and Sachs, F. (1999). Energetic and spatial parameters for gating of the bacterial large conductance mechanosensitive channel, *MscL*. *J. Gen. Physiol.* **113**, 525-540.
- Sukharev, S., Betanzos, M., Chiang, C. S. and Guy, H. R. (2001). The gating mechanism of the large mechanosensitive channel *MscL*. *Nature* **409**, 720-724.
- Tanaka, K., Naruse, K. and Sokabe, M. (2005). *Effects of Mechanical Stresses on the Migrating Behavior of Endothelial Cells*. New Jersey: World Scientific Publishing.
- Tatsumi, H. and Katayama, Y. (1999). Growth cones exhibit enhanced cell-cell adhesion after neurotransmitter release. *Neuroscience* **92**, 855-865.
- Yao, X., Kwan, H. and Huang, Y. (2001). Stretch-sensitive switching among different channel sublevels of an endothelial cation channel. *Biochim. Biophys. Acta* **1511**, 381-390.
- Zenisek, D., Davila, V., Wan, L. and Almers, W. (2003). Imaging calcium entry sites and ribbon structures in two presynaptic cells. *J. Neurosci.* **23**, 2538-2548.
- Zhang, Y., Gao, F., Popov, V. L., Wen, J. W. and Hamill, O. P. (2000). Mechanically gated channel activity in cytoskeleton-deficient plasma membrane blebs and vesicles from *Xenopus* oocytes. *J. Physiol.* **523**, 117-130.
- Zou, H., Lifshitz, L. M., Tuft, R. A., Fogarty, K. E. and Singer, J. J. (2002). Visualization of Ca^{2+} entry through single stretch-activated cation channels. *Proc. Natl. Acad. Sci. USA* **99**, 6404-6409.